

Fixed-frequency space-vector-modulation control for three-phase four-leg active power filters

D. Shen and P.W. Lehn

Abstract: The paper presents a three-dimensional space-vector-modulation scheme for three-phase four-wire active power filters. The focus is on the implementation of a fixed frequency pulse width modulation (PWM) scheme with a minimum number of switch commutations per period and maximum DC bus voltage utilisation. For three-wire applications, space vector modulation is known to provide better utilisation of the DC voltage compared to a sinusoidal PWM approach. This concept is extended to four-wire applications by employing a four-leg active power filter. The largest symmetrical region in which the active filter's voltage space vector may reside is identified. Restricting the voltage space vector to this region avoids over-modulation and thereby prevents the production of low order harmonics. A digital controller is employed to provide deadbeat current control. The combination of the digital controller and the modulation scheme gives the four-leg active power filter the capability to independently track reference current waveforms in the three phases within one switching period. The four-leg active power filter may be used for harmonic compensation, reactive power compensation, load balancing, and neutral current compensation. Experimental results obtained from a 5kVA laboratory active power filter validate the proposed modulation scheme as well as the control design.

1 Introduction

The widespread use of nonlinear loads is leading to a variety of undesirable phenomena in the operation of power systems. The harmonic components in current and voltage waveforms are the most important among these. Conventionally, passive filters have been used to eliminate line current harmonics. However, they introduce resonance in the power system and tend to be bulky. With the improved performance of power and control circuits, active power filters have gradually been recognised as a viable alternative to passive filters.

In many commercial and industrial installations, power is distributed through a three-phase four-wire system. This type of system has unique problems. If nonlinear single-phase loads are present, or the three-phase load is unbalanced, line currents are unbalanced and neutral currents flow. These neutral currents contain both fundamental and harmonic components. In extreme cases, the neutral currents are potentially damaging to both the neutral conductor and the transformer to which it is connected. Three-phase three-wire active power filters cannot adequately reduce or eliminate line harmonics in this situation [1]. To mitigate these problems, three-phase four-wire active filters have been proposed. In [2] a systematic design procedure for a four-wire active power filter with a split-capacitor inverter topology is presented. [3] proposes a four-wire active power filter with a four-leg inverter topology, as depicted in Fig. 1. For the first

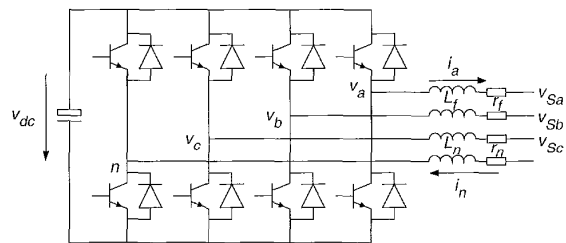


Fig. 1 Four-leg inverter-based active power filter connected to an AC mains

topology, an auxiliary controller must be applied to balance the two DC capacitor voltages. The latter topology only requires regulation of one DC bus voltage and can significantly simplify the control circuit. The latter approach has also been shown to reduce both current and voltage ratings of the DC-side capacitor. Thus the four-leg inverter offers distinct advantages when compared with the three-phase inverter with split DC capacitors.

In a four-leg active filter, the three-phase currents and the neutral current must be controlled. In [4] four independent current controllers are employed for the three phases and the neutral current. Since only three of the four controlled currents are linearly independent, the interaction among the controllers results in either the currents straying outside their tolerance band or the switching frequency straying from its set value. The problem is solved by a space-vector-based current controller in the $\alpha\beta\theta$ coordinate system, as proposed in [5, 6]. These controllers impose equal hysteresis errors in the converter's four-wire currents.

For four-leg active power filters, the current tracking ability is usually provided by a hysteresis-based, tolerance-band controller [3–7]. In hysteresis control, switching

© IEE, 2002

IEE Proceedings online no. 20020377

DOI: 10.1049/ip-epa:20020377

Paper first received 17th October 2001 and in revised form 21st February 2002

The authors are with the Department of Electrical and Computer Engineering, University of Toronto, 10 King's College Road, Toronto, Ontario M5S 3G4, Canada

frequency and harmonic components of the injected current vary with the operating point, making design of the power circuit difficult. A fixed-frequency PWM pattern generator is desirable for all but the smallest converters.

This paper presents a three-dimensional space-vector-modulation scheme using fixed frequency PWM. The benefit of a space-vector approach is a 15% improvement of DC voltage utilisation compared with sinusoidal PWM. Effectively, this improvement is achieved by superimposing zero sequence triple-n harmonic voltages on the sinusoidal PWM reference signals [8]. Unlike in a three-wire system, this zero-sequence converter voltage will cause a zero-sequence current to flow in a four-wire system. It is shown that use of a four-leg converter, along with appropriate selection of the space vectors, can eliminate the zero-sequence-current flow without sacrificing the DC voltage utilisation. All limits on the space vector are determined to ensure over-modulation, and thus the injection of low-order harmonics is avoided. A simple digital controller is designed for the converter based on deadbeat control concepts [9]. The resulting four-leg active filter may be used for harmonics compensation, reactive power compensation, load balancing and neutral current compensation. Depending on the application, one or more of these compensation objectives may be simultaneously achieved. A 5 kVA laboratory system is designed and tested to validate the concepts. Experimental results demonstrate that the active filter can simultaneously meet all four of the above objectives, i.e. eliminate harmonics, compensate reactive power, balance the load and eliminate neutral currents.

2 Three-dimensional space vectors for a four-leg VSI

The states of the switches in inverter legs a , b , c and n are defined by the logic functions S_a , S_b , S_c , S_n . For $S_a=1$, the upper switch of leg a is conducting and the lower switch is blocked; for $S_a=0$ it is the lower switch that is

conducting and the upper is blocked. The same notation applies to legs b , c and n .

The system variables (currents or voltages) are converted to the $\alpha\beta 0$ coordinate system by the transformation defined by (1). In this coordinate system, the zero sequence component is decoupled from the $\alpha\beta$ components.

$$\begin{bmatrix} v_\alpha \\ v_\beta \\ v_0 \end{bmatrix} = \sqrt{\frac{2}{3}} \begin{bmatrix} 1 & -\frac{1}{2} & -\frac{1}{2} \\ 0 & \frac{\sqrt{3}}{2} & -\frac{\sqrt{3}}{2} \\ \frac{1}{\sqrt{2}} & \frac{1}{\sqrt{2}} & \frac{1}{\sqrt{2}} \end{bmatrix} \begin{bmatrix} v_a \\ v_b \\ v_c \end{bmatrix}, \quad (1)$$

$$\begin{bmatrix} i_\alpha \\ i_\beta \\ i_0 \end{bmatrix} = \sqrt{\frac{2}{3}} \begin{bmatrix} 1 & -\frac{1}{2} & -\frac{1}{2} \\ 0 & \frac{\sqrt{3}}{2} & -\frac{\sqrt{3}}{2} \\ \frac{1}{\sqrt{2}} & \frac{1}{\sqrt{2}} & \frac{1}{\sqrt{2}} \end{bmatrix} \begin{bmatrix} i_a \\ i_b \\ i_c \end{bmatrix}$$

Table 1 shows the values obtained for phase-to-neutral voltages and their corresponding $\alpha\beta 0$ variables for all 16 possible switch combinations. The phase-to-neutral voltage is the voltage between the specified phase and the midpoint of the neutral leg.

Distribution of the 16 switching vectors expressed in Table 1 can be represented graphically in Fig. 2. There are two zero switching vectors (0000, 1111) and 14 non-zero switching vectors. Projection of all switching vectors on the $\alpha\beta$ plane forms a hexagon shown in Fig. 3, which is the well known space-vector representation of a conventional three-phase inverter. The projected vectors have a length of $(2/\sqrt{6})v_{dc}$.

In order to visualise the switching vectors in the $\alpha\beta 0$ reference frame, an outline of all these vectors is presented in Fig. 4. It is a hexagonal tube, terminated top and bottom in a three-sided pyramidal shape. The controllable area of the four-leg-inverter output voltage is within this block.

To avoid unwanted lower harmonics in the output voltage, the space-vector control for a conventional three-phase inverter requires the reference voltage vector to be

Table 1: Variable Switch combinations and inverter voltages in abc and $\alpha\beta 0$ coordinates

State	v_a	v_b	v_c	v_α	v_β	v_0
0000	0	0	0	0	0	0
0001	$-v_{dc}$	$-v_{dc}$	$-v_{dc}$	0	0	$-\sqrt{3}v_{dc}$
0010	0	0	v_{dc}	$-\frac{1}{\sqrt{6}}v_{dc}$	$-\frac{1}{\sqrt{2}}v_{dc}$	$\frac{1}{\sqrt{3}}v_{dc}$
0011	$-v_{dc}$	$-v_{dc}$	0	$-\frac{1}{\sqrt{6}}v_{dc}$	$-\frac{1}{\sqrt{2}}v_{dc}$	$-\frac{2}{\sqrt{3}}v_{dc}$
0100	0	v_{dc}	0	$-\frac{1}{\sqrt{6}}v_{dc}$	$\frac{1}{\sqrt{2}}v_{dc}$	$\frac{1}{\sqrt{3}}v_{dc}$
0101	$-v_{dc}$	0	$-v_{dc}$	$-\frac{1}{\sqrt{6}}v_{dc}$	$\frac{1}{\sqrt{2}}v_{dc}$	$-\frac{2}{\sqrt{3}}v_{dc}$
0110	0	v_{dc}	v_{dc}	$-\frac{2}{\sqrt{6}}v_{dc}$	0	$\frac{2}{\sqrt{3}}v_{dc}$
0111	$-v_{dc}$	0	0	$-\frac{2}{\sqrt{6}}v_{dc}$	0	$-\frac{1}{\sqrt{3}}v_{dc}$
1000	v_{dc}	0	0	$\frac{2}{\sqrt{6}}v_{dc}$	0	$\frac{1}{\sqrt{3}}v_{dc}$
1001	0	$-v_{dc}$	$-v_{dc}$	$\frac{2}{\sqrt{6}}v_{dc}$	0	$-\frac{2}{\sqrt{3}}v_{dc}$
1010	v_{dc}	0	v_{dc}	$\frac{1}{\sqrt{6}}v_{dc}$	$-\frac{1}{\sqrt{2}}v_{dc}$	$\frac{2}{\sqrt{3}}v_{dc}$
1011	0	$-v_{dc}$	0	$\frac{1}{\sqrt{6}}v_{dc}$	$-\frac{1}{\sqrt{2}}v_{dc}$	$-\frac{1}{\sqrt{3}}v_{dc}$
1100	v_{dc}	v_{dc}	0	$\frac{1}{\sqrt{6}}v_{dc}$	$\frac{1}{\sqrt{2}}v_{dc}$	$\frac{2}{\sqrt{3}}v_{dc}$
1101	0	0	$-v_{dc}$	$\frac{1}{\sqrt{6}}v_{dc}$	$\frac{1}{\sqrt{2}}v_{dc}$	$-\frac{1}{\sqrt{3}}v_{dc}$
1110	v_{dc}	v_{dc}	v_{dc}	0	0	$\sqrt{3}v_{dc}$
1111	0	0	0	0	0	0

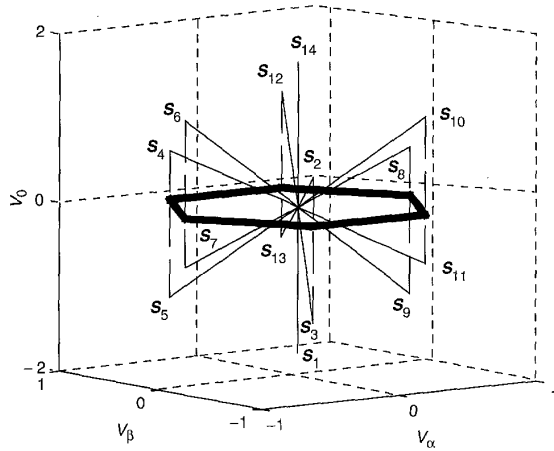


Fig. 2 Switching vectors of a four-leg inverter *a* in $\alpha\beta 0$ coordinates
b projections on the $\alpha\beta$ plane

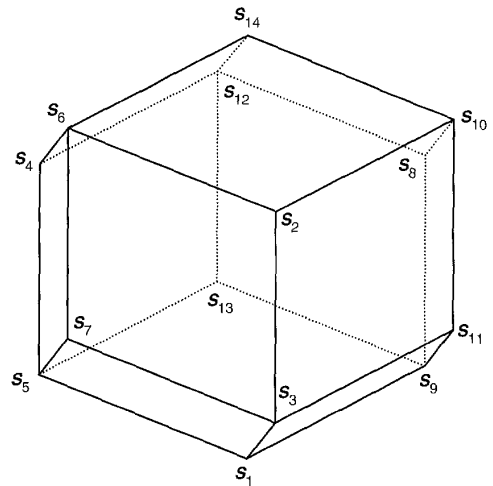


Fig. 4 The controllable area of a four-leg inverter showing the outline of the switching vectors

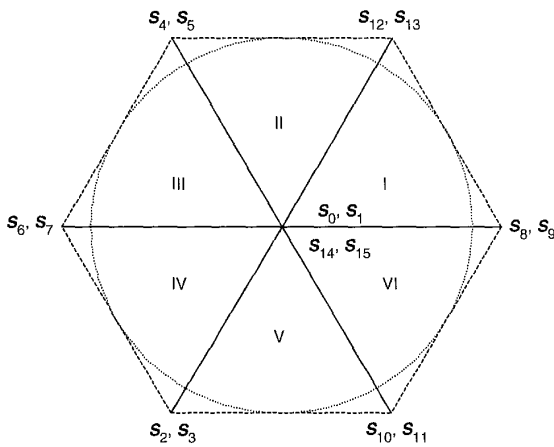


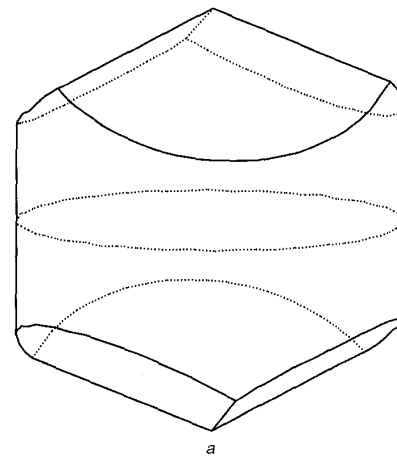
Fig. 3 Switching vectors of a four-leg inverter showing projections on the $\alpha\beta$ plane

located in the inner tangent circle of the hexagon, as included in Fig. 3. The same requirement applies to the space-vector control for a four-leg inverter. With this constraint, the controllable area of the four-leg inverter is depicted in Fig. 5*a*. It is a cylinder terminated top and bottom by three-sided pyramids, where the top pyramid is rotated 60° about the cylinder's axis with respect to the bottom pyramid. The cylindrical shape demonstrates that a zero sequence may be injected without sacrificing any DC voltage utilisation compared to two-dimensional space vector modulation.

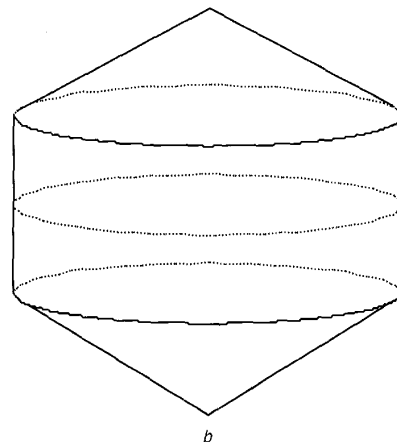
The active filter terminal voltage comprises of two components: one large component that matches the system voltage, and a second incremental component that drives a compensation current into the system. Rotation of the space vector around the 0-axis is required to match the system voltage. To ensure this rotation does not drive the space vector outside the operating region, a conical constraint is applied. This is shown in Fig. 5*b* and expressed mathematically by (2).

$$|v_{\alpha\beta}| \leq \frac{v_{dc}}{\sqrt{2}} \quad (2a)$$

$$\sqrt{2}|v_{\alpha\beta}| + |v_0| \leq \sqrt{3}v_{dc} \quad (2b)$$



a



b

Fig. 5 The controllable area of a four-leg inverter
a the controllable area with $\alpha\beta$ constraint
b the controllable area with all constraints

Constraint (2*a*) is employed to find the DC voltage necessary to yield the required voltage vector amplitude $|v_{\alpha\beta}|$. Constraint (2*b*) then yields the associated bounds on

v_0 . Note that v_0 may have a significantly higher amplitude than either v_α or v_β .

3 Three-dimensional space-vector modulation

The object of space-vector modulation is to synthesise a reference voltage vector through time averaging. The modulation can be divided into two steps: first, select the applied switching vectors and compute the duration time for each switching vector; second, decide the switching sequence of the selected vectors. One 60 degree sector (sector V in Fig. 3) is extracted as an example and shown in Fig. 6.

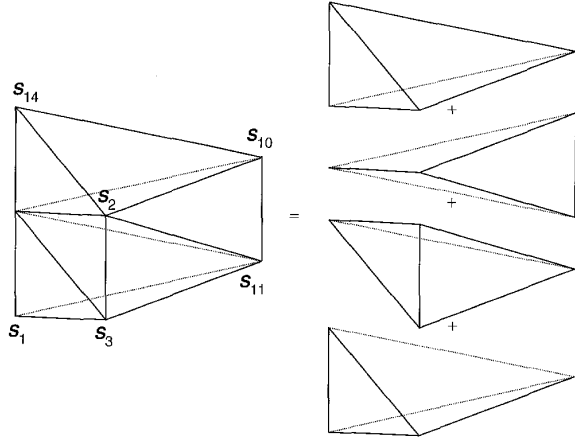


Fig. 6 A 60 degree region and its division into 4 tetrahedrons

3.1 Combination of applied switching vectors

There are six non-zero and two zero vectors available in a 60 degree sector. Often, there are numerous possible combinations of switching vectors that will yield the same time-averaged reference-voltage vector. In $\alpha\beta$ -frame space-vector modulation for a conventional three-phase inverter, two adjacent non-zero vectors, together with zero vectors, are used to synthesise the reference-voltage vector. This approach is used to minimise harmonics. By analogous reasoning, adjacent vectors in $\alpha\beta 0$ coordinates should be identified. The 60 degree sector can be divided into four tetrahedrons from top to bottom, as shown in Fig. 6. Each tetrahedron is defined by three adjacent non-zero vectors and two zero vectors. Any voltage space vector within a tetrahedron may be synthesised by the three vectors making up the tetrahedron and the two zero vectors. The selection of applied switching vectors is broken into two stages: first, the 60 degree sector is identified according to the $\alpha\beta$ values of the reference vector; second, the required tetrahedron is determined according to the zero sequence value of the reference vector.

The 14 non-zero switching space vectors are represented by $\mathbf{S}_i = [v_{\alpha i} \ v_{\beta i} \ v_{0i}]^T$ ($i = 1, 2, \dots, 14$). Assuming the reference voltage vector is $\mathbf{S}_r = [v_{\alpha r} \ v_{\beta r} \ v_{0r}]^T$, the adjacent three non-zero space vectors are $\mathbf{S}_j, \mathbf{S}_k, \mathbf{S}_m$ ($j, k, m \in \{1, 2, \dots, 14\}$), and the corresponding duty cycles are d_j, d_k, d_m . The reference vector is composed from the vectorial time average of the applied space vectors according to (3). This relation may be solved in terms of the duty cycles as in (4).

$$[\mathbf{S}_j \ \mathbf{S}_k \ \mathbf{S}_m] [d_j \ d_k \ d_m]^T = \mathbf{S}_r \quad (3)$$

$$\begin{cases} [d_j \ d_k \ d_m]^T = [\mathbf{S}_j \ \mathbf{S}_k \ \mathbf{S}_m]^{-1} \mathbf{S}_r \\ d_0 = 1 - (d_j + d_k + d_m) \end{cases} \quad (4)$$

where d_0 is the duty cycle of the zero vectors.

3.2 Switching sequence of the selected vectors

For the three-leg converter, two switching sequence schemes were proposed in [10] for the motor drive. For active filter applications, the selected switching vectors should be placed in a sequence, optimised to reduce switching loss by reducing the number of commutations. The number of used zero vectors and the switching sequence of the selected vectors will influence the number of commutations in each sampling period. If two zero vectors are selected and the switching sequence is symmetric in each sampling period, the sequence of vectors applied for the third tetrahedron of sector V is as shown in Fig. 7a. The number of commutations in one sampling period is eight. If two zero vectors are selected and the switching sequence in the adjacent sampling period is alternated, the sequence of vectors is given in Fig. 7b and the commutation number is four. When only one zero vector is used, two possible sequences of vectors exist for the same tetrahedron, depending on the zero vector selected. These two sequences are depicted in Figs. 7c and d. The commutation number in one sampling period is then six. The scheme in Fig. 7b is therefore selected as the preferred switching sequence due to the lower number of commutations.

4 Control design for the 4-leg active power filter

The studied active power filter system is presented in Fig. 8. The digital controller comprises of a DSP current controller and a space vector modulator.

4.1 The inner current controller

In $\alpha\beta 0$ coordinates the system model of the active power filter is:

$$\begin{cases} \frac{di_\alpha}{dt} = -\frac{r_f}{L_f} i_\alpha + \frac{1}{L_f} (v_\alpha - v_{s\alpha}) \\ \frac{di_\beta}{dt} = -\frac{r_f}{L_f} i_\beta + \frac{1}{L_f} (v_\beta - v_{s\beta}) \\ \frac{di_0}{dt} = -\frac{r_0}{L_0} i_0 + \frac{1}{L_0} (v_0 - v_{s0}) \end{cases} \quad (5)$$

where $r_0 = r_f + 3r_n$, $L_0 = L_f + 3L_n$. In digital implementation, using a zero-order hold model of the system and the trapezoid integration rule yields the system equation:

$$\begin{cases} v_{\alpha,k+1} = -v_{\alpha,k} + 2v_{s\alpha,k+1} + \frac{L_f}{T_s} (i_{\alpha,k+2} - i_{\alpha,k}) + r_f (i_{\alpha,k+2} + i_{\alpha,k}) \\ v_{\beta,k+1} = -v_{\beta,k} + 2v_{s\beta,k+1} + \frac{L_f}{T_s} (i_{\beta,k+2} - i_{\beta,k}) + r_f (i_{\beta,k+2} + i_{\beta,k}) \\ v_{0,k+1} = -v_{0,k} + 2v_{s0,k+1} + \frac{L_0}{T_s} (i_{0,k+2} - i_{0,k}) + r_0 (i_{0,k+2} + i_{0,k}) \end{cases} \quad (6)$$

The current i_k is the present current flowing in the circuit and i_{k+2} is the current flowing after two time steps. The current i_{k+2} is a function of the applied inverter voltage v_k, v_{k+1} and the system voltage. The control therefore forces the current to take on the value i_{k+2} after two sampling time steps (equivalent to one switching period). Thus i_{k+2} may be viewed as the reference command that the current will track. Therefore the control law will be:

$$\begin{cases} v_{\alpha,k+1} = -v_{\alpha,k} + 2v_{s\alpha,k+1} + \frac{L_f}{T_s} (i_{\alpha,ref} - i_{\alpha,k}) + r_f (i_{\alpha,ref} + i_{\alpha,k}) \\ v_{\beta,k+1} = -v_{\beta,k} + 2v_{s\beta,k+1} + \frac{L_f}{T_s} (i_{\beta,ref} - i_{\beta,k}) + r_f (i_{\beta,ref} + i_{\beta,k}) \\ v_{0,k+1} = -v_{0,k} + 2v_{s0,k+1} + \frac{L_0}{T_s} (i_{0,ref} - i_{0,k}) + r_0 (i_{0,ref} + i_{0,k}) \end{cases} \quad (7)$$

The system voltage at the next time step $v_{s,k+1}$ is predicted by the past and present values. If the system voltage is balanced, the $v_{s,k+1}$ can be represented by:

$$\begin{cases} v_{s\alpha,k+1} + j \cdot v_{s\beta,k+1} = e^{j\omega_0 T_s} (v_{s\alpha,k} + j \cdot v_{s\beta,k}) \\ v_{s0,k+1} = 0 \end{cases} \quad (8)$$

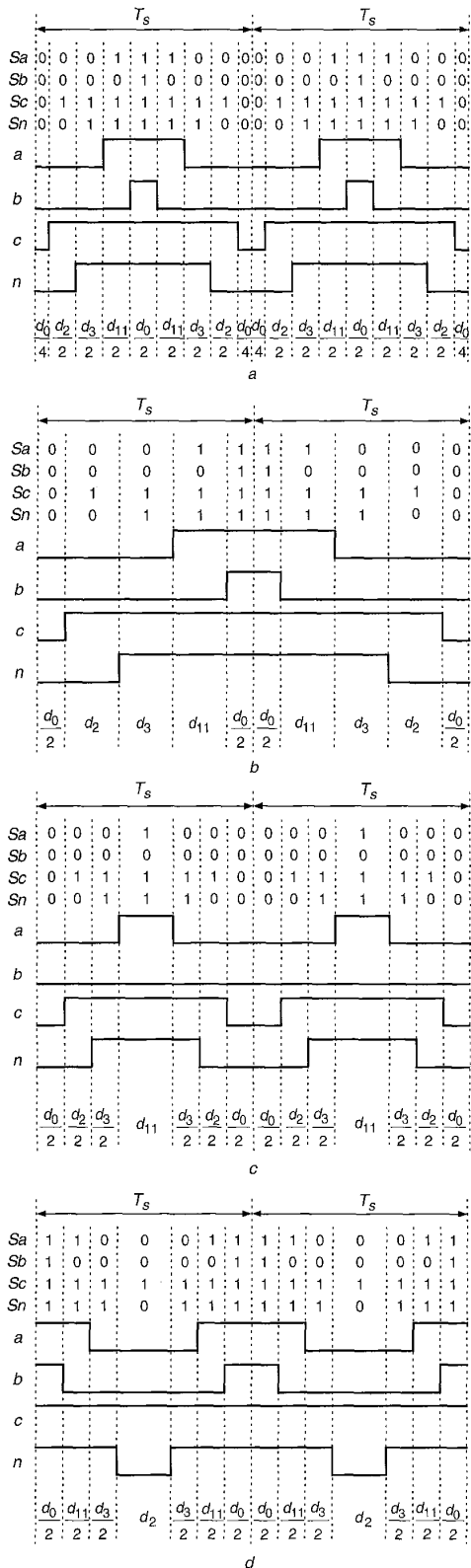


Fig. 7 The switching sequence of the selected vectors (tetrahedron 3 of sector V)

- a Both zero vectors are applied (symmetric)
- b Both zero vectors are applied (asymmetric)
- c Zero vector 0000 is applied
- d Zero vector 1111 is applied

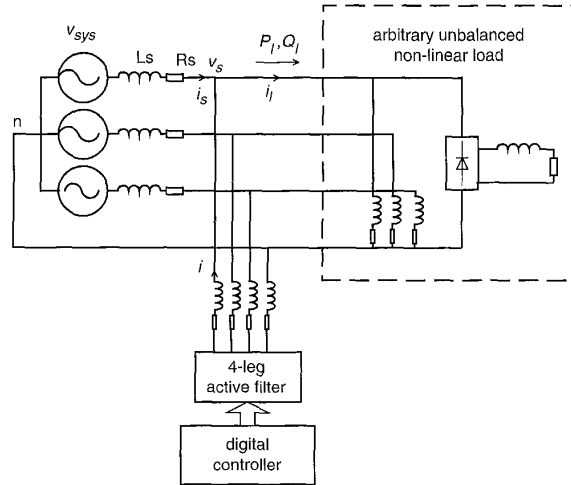


Fig. 8 A four-leg active power filter system

The block diagram of the inner current control loop is given in Fig. 9. The control loop is capable of tracking a step reference change in two sampling steps.

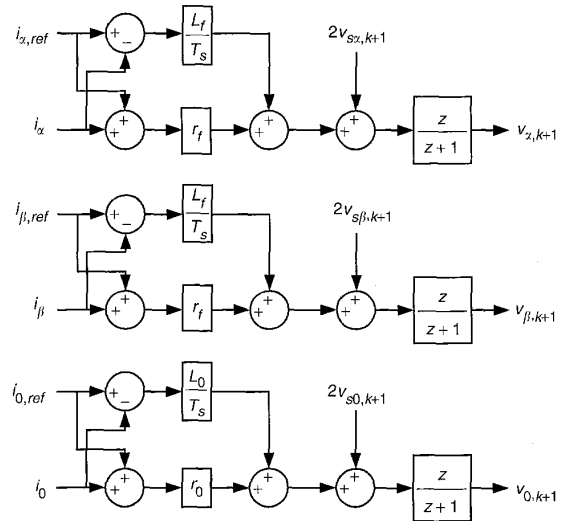


Fig. 9 The block diagram of the inner current-tracking loop

4.2 Creation of the reference current

The outer loop of the control system provides the reference current for the inner current loop. It is depicted in Fig. 10. The outer loop includes a slow PI controller to regulate the DC voltage and a reference current calculation unit. As shown, the active filter provides the entire load current ($i_{\beta s}$, $i_{\beta \beta}$) minus the positive-sequence fundamental current ($i_{\alpha s}$, $i_{\beta \beta}$) necessary to supply the active power in the load and the losses in the active filter. The positive-sequence fundamental current required from the system is calculated from the average required power (\bar{P}), divided by the positive-sequence system voltage ($\bar{v}_{\alpha s}$, $\bar{v}_{\beta \beta}$). A one cycle sliding window DFT calculates the average positive-sequence system voltage.

It should be noted that the two sampling periods delay can cause a significant phase difference between the

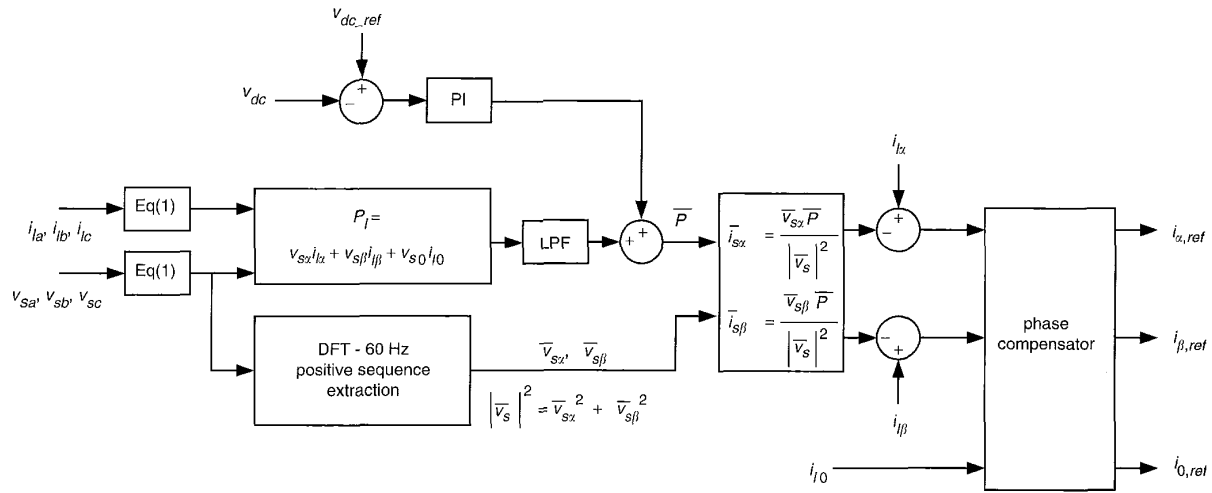


Fig. 10 The block diagram of the outer reference current-control loop

reference and actual currents, especially at harmonic frequencies. To overcome this problem, an equal but opposite phase shift is added to the reference as presented in detail in [11]. This task is performed in the phase-compensation unit.

5 Experimental results

Experimental tests on a 5kVA four-leg IGBT active power filter are carried out to verify the modulation scheme as well as the controller design. The laboratory system is depicted in Fig. 8, where the digital controller is composed of a TMS320C40 DSP-based current controller and a space vector modulator implemented in an FPGA. The filter currents are controlled with the digital controller presented in Figs. 9 and 10. The load includes a balanced three-phase RL load and a single-phase rectifier, connected between phase A and the neutral line. The parameters for the laboratory system are given in the Appendix (Section 8).

Fig. 11 presents the reference currents and sampled output currents of the active filter in $\alpha\beta 0$ coordinates. The sampled currents have the same waveforms as the reference values except for the two-sampling-periods delay. Thus it may be concluded that the deadbeat current controller is operating as anticipated.

The experiment confirms the current tracking ability of the controller. Figs. 12 and 13 give the sampled phase currents and neutral line current waveform with and without the active power filter. The phase A system voltage is also included to show the phase angle between the voltage and current. Without the active power filter, the system currents are composed of undesired reactive currents, unbalanced fundamental currents and unbalanced harmonic components. In this condition, the neutral line carries a quasi-square-wave current required by the single-phase rectifier. When the active power filter is engaged, the system only supplies a fundamental positive sequence current and all other unwanted components are provided by the four-leg active power filter. Fig. 14 depicts the actual phase-A system current taken from an oscilloscope, and the harmonic analysis result is shown in Fig. 15. From the harmonic analysis, it is clear that the low-order harmonic components in the load current are effectively compensated by the active power

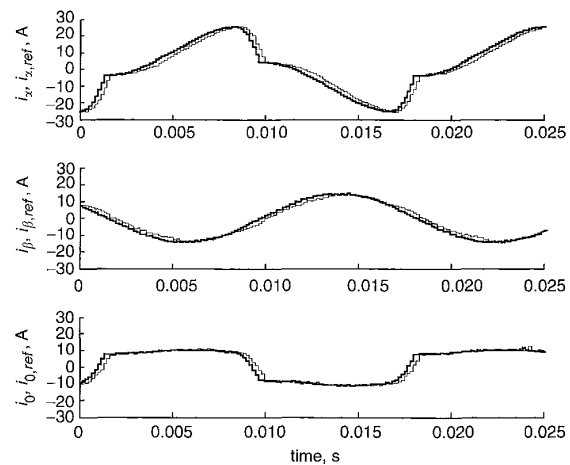


Fig. 11 The reference and sampled currents of the active filter (reference values are in bold, sampled currents lag reference values)

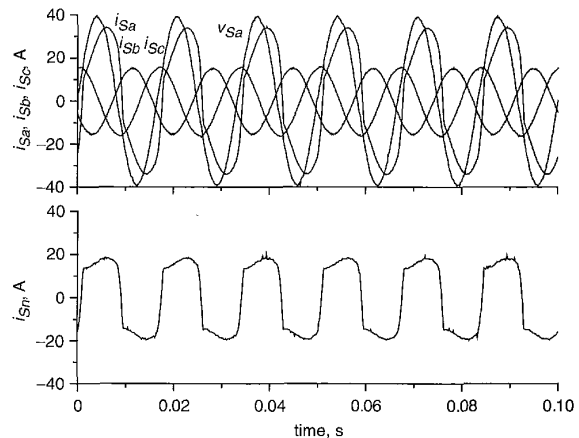


Fig. 12 The system current waveforms result without active power filter

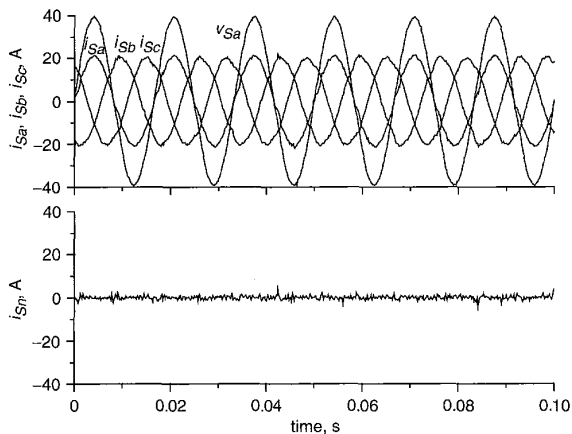


Fig. 13 The system current waveforms with active power filter

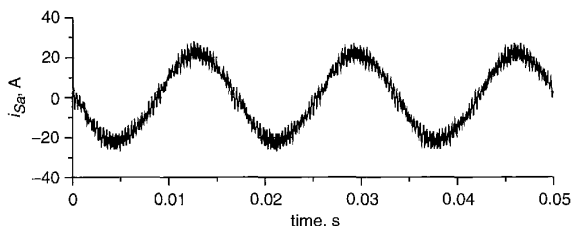


Fig. 14 The actual waveform of the phase A current

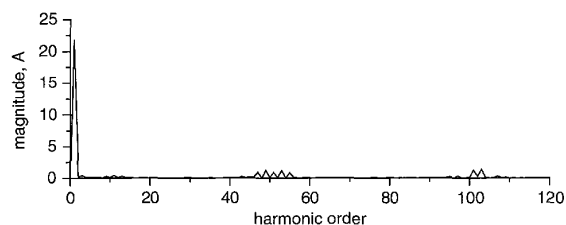


Fig. 15 The harmonic analysis result

filter. The residual high-order harmonics in the system current are caused by the converter switching. Since fixed frequency PWM is employed, these harmonics are always centred around the converter switching frequency, and can be easily filtered out with a tuned passive filter of low rating.

6 Conclusion

Four-leg active power filters are especially suitable for power quality improvement in three-phase four-wire systems. For four-leg active power filters, the current tracking ability is typically provided by a hysteresis-based, tolerance-band controller. In contrast, this paper presents a three-dimensional space-vector-modulation scheme that

employs fixed frequency PWM. Appropriate selection of the switching vectors is shown to yield both high DC voltage utilisation and a significant reduction in the number of switch commutations per period. Converter control is performed in the $\alpha\beta 0$ coordinate frame using digital deadbeat control. The combination of the digital controller and the three-dimensional space-vector-modulation scheme offers the capability to track the reference current waveforms in two sampling periods. The proposed four-leg active power filter may be used for current harmonic compensation, reactive power compensation, load balancing and neutral current compensation. Experimental results obtained from a 5 kVA laboratory active power filter validate the proposed modulation scheme as well as the control design.

7 References

- THOMAS, T., HADDAD, K., JOOS, G., and JAAFARI, A.: 'Performance evaluation of three phase three and four wire active filters'. Conference Record of the IEEE IAS Annual Meeting, San Diego, CA, USA, 1996, pp. 1016-1023
- HADDAD, K., THOMAS, T., JOOS, G., and JAAFARI, A.: 'Dynamic performance of three phase four wire active filters'. Proceedings of IEEE APEC'97, Atlanta, Georgia, USA, 1997, pp. 206-212
- QUINN, C.A., and MOHAN, N.: 'Active filtering of harmonic currents in three-phase four-wire system with three-phase and single-phase nonlinear loads'. Proceedings of IEEE APEC'92, Boston, Massachusetts, USA, 1992, pp. 829-836
- QUINN, C.A., MOHAN, N., and MEHTA, H.: 'A four-wire current-controlled converter provides harmonic neutralization in three-phase four-wire system'. Proceedings of IEEE APEC'93, San Diego, CA, USA, 1993, pp. 841-846
- VERDELHO, P., and MARQUES, G.D.: 'Four-wire current-regulated PWM voltage converter', *IEEE Trans. Ind. Electron.*, 1998, **45**, pp. 761-770
- VERDELHO, P., and MARQUES, G.D.: 'A current control system based on $\alpha\beta 0$ variables for a four-leg PWM voltage converter'. Proceedings of IEEE IECON'98, Aachen, Germany, 1998, pp. 1847-1852
- SINGH, B., ANURADHA, A., KOTHARI, D.P., and CHANDRA, A.: 'Variable structure control of four pole voltage source inverter for active filtering of nonlinear loads in 3-phase 4-wire systems'. Conference Record of IEEE Power Quality'98, Hyderabad, India, 1998, pp. 89-94
- HOLTZ, J.: 'Pulsewidth modulation—a survey', *IEEE Trans. Ind. Electron.*, 1992, **39**, pp. 410-420
- HOLMES, D.G., and MARTIN, D.A.: 'Implementation of a direct digital predictive current controller for single and three phase voltage source inverters'. Conference Record of the IEEE IAS Annual Meeting, 1996, pp. 906-913
- STEFANOVIC, V.R., and VUKOSAVIC, S.N.: 'Space-Vector PWM Voltage Control with Optimized Switching Strategy'. Conference Record of the IEEE IAS Annual Meeting, 1992, pp. 1025-1033
- SVENSSON, J., and OTTERSTEN, R.: 'Shunt active filtering of vector current-controlled VSC at a moderate switching frequency', *IEEE Trans. Ind. Appl.*, 1999, **35**, pp. 1083-1089

8 Appendix

PWM specifications

switching frequency = 3.06 kHz

sampling frequency = 6.12 kHz

Active-filter specifications

KVA = 5.0 kVA

$V_b = 110$ V

$L_f = 0.64$ mH (0.10 pu)

$L_n = 1.0$ mH (0.156 pu)

Load parameters

3-phase: $R_{ac} = 8.0 \Omega$, $X_{ac} = 10.0 \Omega$

1-phase rectifier: $R_{dc} = 4.2 \Omega$